Continuous wave second-harmonic generation using domain-disordered quasi-phase matching waveguides

Sean J. Wagner,[1,a)] Barry M. Holmes,[2] Usman Younis,[2] Amr S. Helmy,[1] J. Stewart Aitchison,[1] and David C. Hutchings[2]
[1]*Edward S. Rogers Sr. Department of Electrical and Computer Engineering, University of Toronto, 10 King's College Road, Ontario M5S 3G4, Canada*
[2]*Department of Electronics and Electrical Engineering, University of Glasgow, Glasgow, G12 8QQ Scotland, United Kingdom*

(Received 3 February 2009; accepted 25 March 2009; published online 14 April 2009)

Second-harmonic generation in domain-disordered quasi-phase-matched GaAs/AlGaAs superlattice-core waveguides was demonstrated using a continuous wave fundamental source. Output second-harmonic powers of up to 1.6 μW were measured when on a Fabry-Pérot resonance peak. Temperature-related bistable behavior was observed in both the fundamental and second-harmonic output when tuning either the input power or input wavelength. © *2009 American Institute of Physics*. [DOI: 10.1063/1.3119629]

Semiconductor-based nonlinear optical waveguides have opened up the possibility of creating compact, monolithically integrated, and efficient frequency conversion devices. The AlGaAs material system is of particular interest for its mature fabrication technology and large nonlinear optical coefficients. However, phase matching second-order nonlinear wave mixing processes is challenging due to the absence of any natural birefringence in the material. This makes it difficult to achieve phase matching required for continuous frequency conversion. Several approaches have been demonstrated to overcome this problem including the use of artificial form birefringence,[1,2] modal phase matching,[3] Bragg reflection waveguides,[4] and domain-reversal quasi-phase matching.[5] These methods have several drawbacks including high optical losses, fabrication complexity, and poor integration potential with active devices such as pump lasers.

Another method to achieve phase matching is to use domain-disordered quasi-phase matching (DD-QPM) waveguides. In this approach, a semiconductor superlattice structure is periodically altered by quantum-well intermixing (QWI)[6] along the propagation direction. This modulates the energy band gap of the superlattice and, correspondingly, the magnitude of the second-order nonlinear coefficient $\chi^{(2)}$. It is predicted that the modulation in the large bulklike $\chi^{(2)}_{xyz}$ coefficient in AlGaAs superlattice structures can exceed 100 pm V^{-1}.[7] Second-harmonic generation (SHG) has been demonstrated previously in DD-QPM superlattice waveguides using ultrafast pulsed laser systems for pumping.[8] Since then, significant improvements have been made in fabrication processes yielding waveguides with low scattering loss such that the high peak powers only available from pulsed sources are not necessary to observe SHG. In this letter, we demonstrate SHG in a GaAs/AlGaAs superlattice-core DD-QPM waveguide using a continuous wave source.

The waveguide structure consisted of a 0.6-μm-thick core layer of 14:14 monolayer GaAs/$Al_{0.85}Ga_{0.15}As$ superlattice. On either side were 0.3-μm-thick buffer layers of $Al_{0.56}Ga_{0.44}As$ and 0.8-μm-thick $Al_{0.60}Ga_{0.40}As$ cladding layers. A 1.0-μm-thick base layer of $Al_{0.85}Ga_{0.15}As$ was added below the lower cladding layer to isolate the optical modes from the substrate. All layers were grown on a semi-insulating GaAs substrate by molecular beam epitaxy. QPM gratings were formed by patterned QWI of the superlattice using ion-implantation. An implantation mask was formed by electroplating of a 2.3-μm-thick gold layer for a QPM grating period of 3.5 μm and a 60:40 duty cycle (60% masked). Ion implantation was carried out using 4.0 MeV As^{2+} ions at a dosage of 2.0×10^{13} cm^{-2} followed by rapid thermal annealing at a temperature of 775 °C for 60 s. Photoluminescence measurements at 77 K showed a band gap energy blueshift of 76 nm in the intermixed regions of the sample. Rib waveguides 3.5 μm wide and 1.0 μm deep were fabricated by electron beam lithography and reactive ion etching. The final sample was cleaved to a length of 3.5 mm.

The waveguides were characterized using a tunable continuous wave C-band laser with a 100 kHz linewidth followed by an erbium-doped fiber amplifier to boost the power up to 350 mW. The beam was TE polarized to induce Type-I SHG in the waveguides. Light was end-fire launched into the waveguides using an antireflection-coated 40× objective and was collected at the output using a 20× microscope objective. The output second-harmonic (SH) power was detected using a silicon photodetector. Linear optical losses at wavelengths between 1540 and 1570 nm measured by the Fabry-Pérot method averaged 0.9 cm^{-1}. The free-spectral range at the fundamental wavelength was measured to be 0.10 nm.

Internal SH powers of up to 1.6 μW were determined after accounting for the end facet reflectivity of the waveguides and the collection efficiency of the output objective lens. The internal fundamental power is enhanced by the Fabry-Pérot cavity formed by the waveguide facets. By accounting for the linear losses of the waveguides, the internal enhancement in the fundamental power at the input facet was calculated to be up to 46%. For an optical power of 310 mW measured after the input objective lens, the internal fundamental power was deduced to be about 84 mW just after the input facet (deduced by measuring the transmitted fundamental). The normalized internal conversion efficiency

a)Electronic mail: sean.wagner@utoronto.ca.

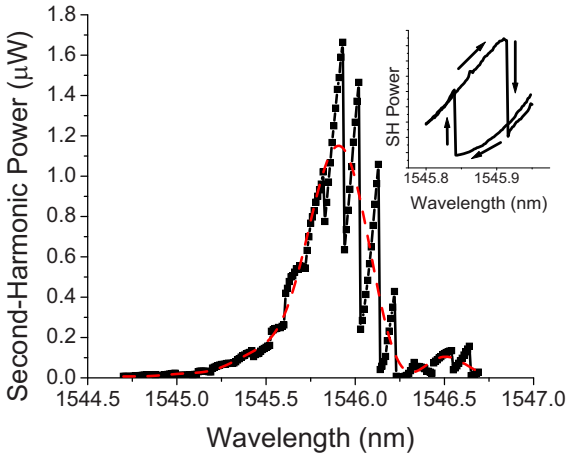

FIG. 1. (Color online) SHG tuning curves for waveguide with a 3.5 μm QPM period recorded by scanning from short-to-long wavelengths (increasing scan, black solid). The dotted red curve shows the increasing wavelength scan after low pass filtering of the data to remove the Fabry-Pérot features. The inset shows a tuning hysteresis loop around a single Fabry-Pérot feature.

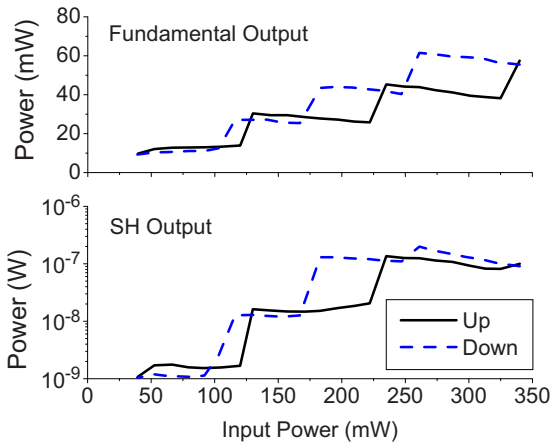

FIG. 3. (Color online) Output fundamental power (top) and second-harmonic power (bottom) at the detectors as the input power is increased (up curve) and decreased (down curve) at a fundamental wavelength of 1545.41 nm. Note that due to the nonlinear dependence, the second-harmonic power is shown on a logarithmic scale.

was therefore calculated to be 0.18 % W^{-1} cm^{-2}.

Scans of the fundamental wavelength were performed around the phase-matching wavelengths for each QPM period. The scan interval was 0.01 nm with a three second delay added between scan points. The tuning curve for an increasing wavelength scan is shown in Fig. 1 with the phase-matching peak located around 1545.9 nm. The Fabry-Pérot features were asymmetric with the short wavelength sides being gradual and the long wavelength sides exhibiting sharp drops. Similar asymmetric features were also observed in the transmitted fundamental. Performing the scan for decreasing wavelength did not provide an overlapping characteristic, but nevertheless also demonstrated similar asymmetric features. By limiting the wavelength scan to less than the free-spectral range, a bistable hysteresis loop was obtained when tuning back and forth with a reduced scan interval of 0.002 nm, as shown in the inset of Fig. 1. Also shown in Fig. 1 is the tuning curve with the Fabry-Pérot features removed by low pass filtering of the data. This curve resembles the sinc^2 shape consistent with phase-matched SHG processes. The full width at half maximum bandwidth is 0.45 nm. Figure 2 shows these filtered tuning curves for a range of fundamental beam powers. The phase-matching peak wavelength shifts to longer wavelengths with increasing optical power levels. This indicated changes to the effective refractive index of the waveguide, which alters the phase-matching condition.

In another experiment, the output second harmonic and transmitted fundamental powers were recorded at a fixed wavelength of 1545.41 nm as the fundamental beam power was increased from 40 to 340 mW, and then decreased back to 40 mW. Several hysteresis loops were observed, as shown in Fig. 3, with the switching points occurring simultaneously for both the SH and the fundamental.

The temporal responses of the output second harmonic and fundamental wavelengths were measured to gain further insight into the origin of the bistability. The input beam was first blocked to reduce the power to zero, and then was unblocked thus giving a nearly instantaneous input power ramp up. In all cases, the input power was set to a level above the threshold level of the highest hysteresis loop. The changes in the output second harmonic power are shown in Fig. 4 over a period of 10 s for different input power levels. Three peaks are reached over the course of the temporal response, which corresponds to the number of threshold points in the power up ramp of Fig. 3. The time required to reach steady state

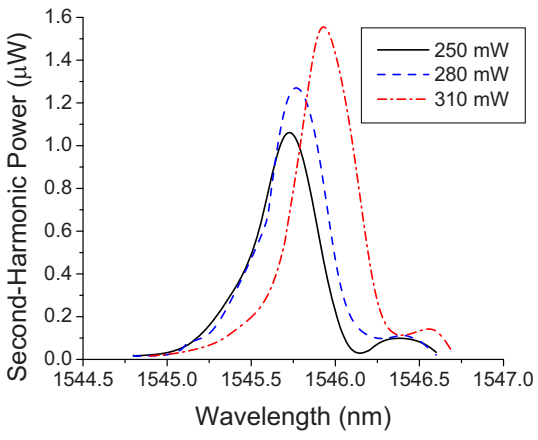

FIG. 2. (Color online) SHG tuning curve envelopes for different input powers.

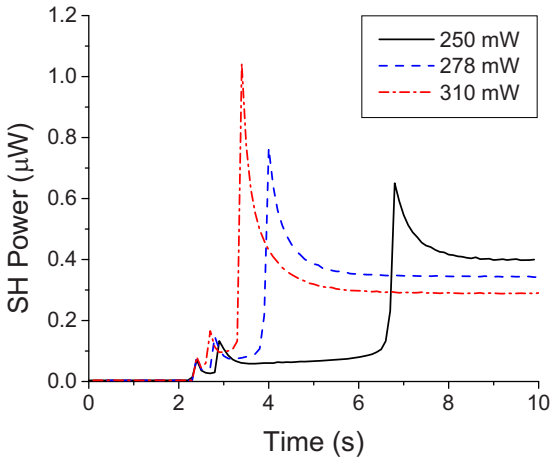

FIG. 4. (Color online) Temporal response at 1545.90 nm for different input power levels above highest threshold level in Fig. 3.

was as long as 6 s for the lowest input power. As the power is increased, the time delay to reach each of the peaks is reduced by as much as 3.4 s at 310 mW compared to 250 mW. This behavior is indicative of a critical slowing down dynamic, well-known in optical bistability.[9]

The bistable behavior can be explained as a shift in the longitudinal cavity modes by changes to the effective index of the waveguide. To shift by Δm modes, the index change required is $\Delta n = n[\Delta m/m]$ where m is the mode number for a particular wavelength. At 1550 nm, this gives an index shift in 2.2×10^{-4}. Thermo-optical effects are attributed as the cause of the observed bistability and shifts in the phase-matching wavelength. The observed behavior and timescales is consistent with whole sample heating as observed previously in bulk AlGaAs waveguides.[10] For the equivalent bulk AlGaAs composition, the thermo-optic coefficient $\partial n/\partial T$ was calculated to be around 1.7×10^{-4} K^{-1} using the Gehrsitz model[11] at 1550 nm. For the calculated Δn, a temperature change of 1.3 K would be sufficient to shift by one longitudinal mode. Bistable behavior in the transmitted fundamental was observed outside the phase-matching bandwidth and in as-grown superlattice waveguides without QPM gratings, and therefore SHG does not play a significant role in the bistability. The sample heating is overwhelmingly dominated by the linear optical loss of the fundamental (which may be attributed to impurities, defects and free-carrier absorption of the residual background doping). Although this loss was measured as 0.9 cm^{-1}, in such a relatively long waveguide sample the absorbance is calculated to be 64% of the transmittance, which corresponds to several 10 s of milliwatts of absorbed power.

The optimal length for the device for SHG is around the smaller of the absorption lengths for the fundamental and the second harmonic. In the present case the second-harmonic loss coefficient was estimated at 20–30 cm^{-1} which suggests that the present 3.5 mm device is significantly longer than optimal. Addressing further improvements in the QPM grating and waveguide fabrication processes will therefore facilitate a higher conversion efficiency in devices of the current length or longer.

In conclusion, we have demonstrated continuous wave SHG in a DD-QPM waveguide based on a GaAs/AlGaAs superlattice core. Output second-harmonic powers reached as high as 1.6 μW and the conversion bandwidth was 0.45 nm. Hysteresis loops from input power and wavelength tuning were observed in both the SH and fundamental. Shifts in the phase-matching wavelength at high powers indicated a change in the effective index of the waveguides. The resulting bistable behavior was deduced to be caused by the thermo-optic effect due to linear optical absorption of the fundamental.

We thank the University of Surrey Ion Beam Centre for carrying out the ion implantation. We also acknowledge the efforts by the technical support staff of the James Watt Nanofabrication Centre at the University of Glasgow.

[1] K. Moutzouris, S. V. Rao, M. Ebrahimzadeh, A. D. Rossi, V. Berger, M. Calligaro, and V. Ortiz, Opt. Lett. **26**, 1785 (2001).
[2] L. Scaccabarozzi, M. M. Fejer, Y. Huo, S. Fan, X. Yu, and J. S. Harris, Opt. Lett. **31**, 3626 (2006).
[3] K. Moutzouris, S. V. Rao, M. Ebrahimzadeh, A. De Rossi, M. Calligaro, V. Ortiz, and V. Berger, Appl. Phys. Lett. **83**, 620 (2003).
[4] B. Bijlani, P. Abolghasem, and A. S. Helmy, Appl. Phys. Lett. **92**, 101124 (2008).
[5] X. Yu, L. Scaccabarozzi, A. C. Lin, M. M. Fejer, and J. S. Harris, J. Cryst. Growth **301–302**, 163 (2007).
[6] J. H. Marsh, Semicond. Sci. Technol. **8**, 1136 (1993).
[7] D. Hutchings, IEEE J. Sel. Top. Quantum Electron. **10**, 1124 (2004).
[8] K. Zeaiter, D. C. Hutchings, R. M. Gwilliam, K. Moutzouris, S. V. Rao, and M. Ebrahimzadeh, Opt. Lett. **28**, 911 (2003).
[9] B. S. Wherrett and D. C. Hutchings, in *Nonlinear Optics in Signal Processing*, edited by R. W. Eason and A. Miller (Chapman and Hall, London, UK, 1993), pp. 145–189.
[10] J. S. Aitchison, J. D. Valera, A. C. Walker, S. Ritchie, P. M. Rodgers, P. McIlroy, and G. I. Stegeman, Appl. Phys. Lett. **51**, 561 (1987).
[11] S. Gehrsitz, F. K. Reinhart, C. Gourgon, N. Herres, A. Vonlanthen, and H. Sigg, J. Appl. Phys. **87**, 7825 (2000).